Int. J. Heat Mass Transfer. Vol. 12, pp. 895–913. Pergamon Press 1969. Printed in Great Britain

THE MICROLAYER IN NUCLEATE POOL BOILING

M. G. COOPER

Engineering Department, University of Cambridge, England

and

A. J. P. LLOYD

Commercial Airplane Division, The Boeing Company, Seattle, Washington, U.S.A.

(*Received* 5 *July* 1968 *and in revised form* 30 *January* 1969)

Abstract—Experiments are reported in which organic liquids underwent pool boiling at low pressure, forming large vapour bubbles on the surface of a heater plate consisting of glass or ceramic. The temperature at the surface of the heater was measured, leading to support for the hypothesis that a thin layer of liquid (the microlayer) forms beneath the vapour bubble.

From the experimental observations it is possible to deduce the thickness of the microlayer, which can also be predicted from a simple theory for the hydrodynamics of the formation of the layer. Experiment and theory agree within ±25 per cent for the limited cases available.

The rates of growth of the bubbles are shown to be of the same order as the rates of evaporation from the microlayers, which can be expressed in analytic form under certain assumptions. A computer program for bubble growth allowing for the microlayer and other factors has been developed and applied to two bubbles growing under widely different bulk temperatures. The predicted radii are within ±15 per cent of those observed.

The relative magnitudes of stresses due to inertia, surface tension, viscosity and gravitation are determined for a typical bubble, and discussed in relation to bubble shape and microlayer formation.

It is stressed that these results may not apply to widely different conditions of boiling.

NOMENCLATURE

A, area;
C_1, constant in $R = C_1 t^n$;
C_2, constant in $\delta_0 = C_2(\nu t_g)^{\frac{1}{2}}$;
C_3, C_4, C_5, constants in Appendix B;
g, local acceleration of gravity;
h_{fg}, latent heat of vaporisation;
k, conductivity;
n, constant in $R = C_1 t^n$;
p, pressure;
P, pressure term (section 5.1);
$\dot{q}$, rate of flow of heat;
$(\dot{q}/A)$, heat flux;
r, radius;
R, radius of bubble;
t, time (suffices e for evaporation, g for growth);
T, temperature (suffices b for bulk liquid, *int* for interface, *sat* for saturation, w for wall);
U, velocity (suffices b for bubble, w for wall);
V, volume;
x, distance parallel to wall;
y, distance normal to wall.

Greek symbols

α, thermal diffusivity of liquid;
δ, thickness of microlayer;
δ_0, initial thickness of microlayer;
θ_d, displacement thickness of boundary layer;
θ_T, thickness of thermal boundary layer;
μ, viscosity of liquid;
ν, kinematic viscosity of liquid;
ρ, density (suffices l for liquid, v for vapour);
σ, interfacial tension.

1. INTRODUCTION

TO EXPLAIN the high heat transfer rates and the behaviour of vapour bubbles during boiling, various mechanisms have been proposed. The aim of the work described here was to shed light upon these mechanisms by determining and analysing the variation with time and position of the heat flux from a heated wall into a boiling liquid.

The experimental work was in continuation of that described by the present authors [1], in which the temperature at the interface between a heated solid and a boiling fluid was determined as a function of time and position. The initial distribution of temperature within the solid was known from other boundary conditions, so the equation for the time varying conduction of heat in the wall could be solved, giving the heat flux at the interface as a function of time and position. Some results were reported in [1], which also briefly surveyed the previous work of Hsu and Schmidt [2], Moore and Mesler [3], Rogers and Mesler [4], Hendricks and Sharp [5] on measurements of temperatures at or near the surface of the solid and the work of Snyder and Edwards [6], Moore and Mesler [3], Sharp [7], Torikai *et al.* [8], Hospeti and Mesler [9] relating to formation of a thin layer of liquid (the microlayer) under a bubble growing on a solid surface. Further evidence of microlayer formation has also been given by Katto and Yokoya [10] and Bonnet *et al.* [11].

This paper describes further results of the general type described in [1] and also discusses the hydrodynamics of formation of microlayers and the effect of evaporation of microlayers upon growth of bubbles, arriving at simple approximate theories.

2. APPARATUS

The apparatus is sketched in Fig. 1 and consisted of a pool boiling vessel, evacuated by means of a rotary pump and condenser, and heated from below, largely by radiation. The base of the vessel was a flat sheet of glass or ceramic, and when it was glass a layer of silver

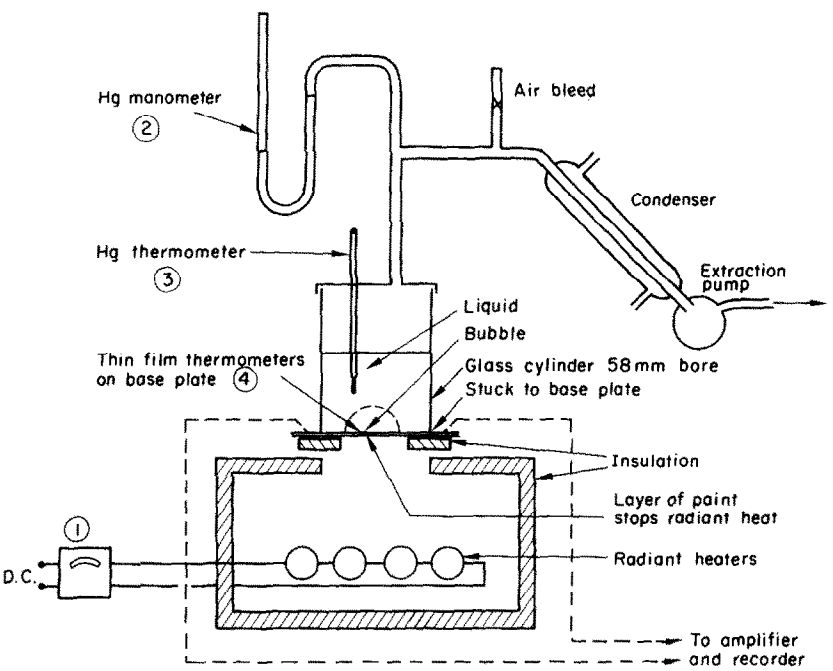

FIG. 1. Functional sketch of apparatus.

paint was applied to its undersurface to prevent transmission of radiation into and through the glass.

The instruments used were:

(1) Electrical instruments for heater input, calibrated for heat flux onto the vessel base,
(2) mercury manometer for system pressure,
(3) mercury in glass thermometer for bulk liquid temperature,
(4) thin film resistance thermometers for the temperature at the interface between the heated base and the fluid.

The thin film thermometers were made using techniques of microcircuitry as described by the authors in [12]. They were sufficiently small (down to 0·075 mm square), closely spaced (down to 0·25 mm), accurate and robust, and being thin (typically 0·25 to 0·5 μm) they had sufficiently short time constants (of order 10^{-8} sec) to follow the local temperature transients while causing no significant perturbation in the flow of heat or fluid. A typical pattern contained six circuits, each consisting of a germanium element 0·1 mm square and two connecting leads running from opposite sides of the element out to conveniently placed soldering tags. The elements were arranged in a straight line at pitch intervals 0·5, 1·5, 1·5, 1·5, 0·5 mm. The four central circuits would normally be used as thermometers, and one of the two outer circuits would be used to initiate a bubble when conditions were suitable, by passing a short current pulse through it. This local heating was less than 10^{-4}J, and did not appear to affect the neighbouring thermometer. The electrical characteristics of the instrument and the associated matching electronics and high speed recorder were described in [1, 12]. The main limitations of the response of the equipment arose from the galvanometers, which had natural frequencies of 1650 Hz, and the accuracy of reading time on the recorder chart, which was about 10^{-3} s. Cine cameras of high speed and of normal speed were also used.

If the thermometers were covered by a protective layer their response times would be impaired, due to the thermal diffusion time of that layer. Layers a few times 10^{-6} m thick would have significant effect. In principle this could be compensated for, by more elaborate analysis of the heat conduction, but that would reduce accuracy, particularly due to uncertainty about the thickness and properties of the layer. In the work reported here, bare thermometers were used, so the fluid had to be a poor electrical conductor. Several organic fluids are suitable, and toluene and isopropyl alcohol were used.

3. EXPERIMENTAL PROCEDURE

The purpose of each experimental run was to produce a single individual vapour bubble, starting from a known position at a known time, and observe its growth and departure and the variation of temperature at the solid surface beneath it. It was not intended to obtain many such runs, and about 100 useful runs were obtained at a typical rate of three or four per working day. For 12 of these runs, simultaneous high speed cine photographs were obtained.

Details of experimental procedure and tests for consistency are given in [1, 13].

4. RESULTS

Figure 2(a) shows sketches of high speed cine photographs at the times indicated during growth and departure of a typical bubble of toluene vapour from a glass plate. Figure 2(b) shows the temperature time curves for that same bubble, using thermometers spaced as described in section 2. For single bubbles of toluene on ceramic plate, or of isopropyl alcohol on glass plate, broadly similar results were obtained. Further details of some early runs are given in [1]. Runs were made covering all combinations of the three heat flux rates, three system pressures, and three bulk liquid temperatures for toluene on glass, for isopropyl alcohol on glass and for toluene on ceramic, with some additional tests to check repeatability and symmetry and a few tests with different spacings of thermometers. Further details are given in [13].

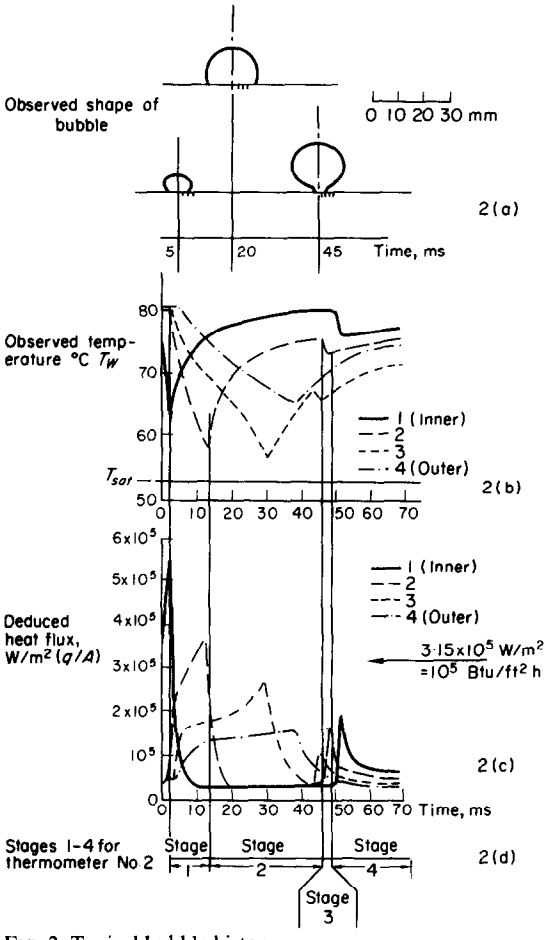

FIG. 2. Typical bubble history.
(a) Shape (from cine film).
(b) Wall temperatures at four thermometers.
(c) Deduced heat fluxes at four thermometers.
(d) Subdivision into stages, for thermometer no. 2.

5. DISCUSSION OF RESULTS

Only those runs with high speed cine films will be discussed in detail. For the other runs, the temperature–time traces were processed by using equation (2) below and checked for conformity to the pattern of variation with experimental parameters, as discussed in [1].

5.1 *Thermodynamics of microlayer evaporation*

The temperature–time curves were processed by numerical integration of the equation for conduction of heat in the wall, to determine the heat flux from the solid to the fluid. Comparison of results of one-dimensional and two-dimensional analysis showed that a one-dimensional analysis by the Runge–Kutta method was generally adequate, but it did not give full details during rapid temperature variation. Applying the one-dimensional analysis to the temperature–time curves of Fig. 2(b) gives the results shown in Fig. 2(c).

From comparison with the cine photographs, it appears that the heat flux at a point remains unchanged until the bubble has grown out over that point, and thereafter it varies in four main stages. For thermometer no. 2 these stages are indicated at the bottom of Fig. 2(d). In some cases two stages are missing. In all cases the final stage starts when the bubble lifts off the thermometer site.

In [1] these variations in heat flux are shown to be consistent with the hypothesis of Snyder and Edwards [6], and Moore and Mesler [3], that a thin layer of liquid (the microlayer) is left against the solid wall as the bubble grows. Such a layer would evaporate during stage 1, leaving the wall dry during stage 2, then stage 3 would be due to the return of liquid as the bubble departs and stage 4 due to the subsequent re-establishment of the thermal boundary layer. At a point where the layer does not evaporate completely, stage 4 interrupts stage 1, so stages 2 and 3 do not occur.

On this hypothesis, the initial thickness δ_0 of the microlayer at a point where temperature is measured can be determined in several ways. The agreement between the results of different methods of calculation is not exact, but it is sufficiently close to lend support to the hypothesis. Table 1 summarizes the results of the calculations. Details are given in [13] but the outline of the methods are as follows:

Table 1, *col.* 3: for cases in which the microlayer is completely evaporated during stage 1, the area under the graph of Fig. 2(c) during stage 1 gives the heat supplied from the wall during evaporation, which is nearly the latent

Table 1. Microlayer thickness δ_0

Run ref.	Radius to thermometer (mm)	δ_0 deduced from experimental results: from heat flow, in solid (μm)	δ_0 deduced from experimental results: from heat flow, in liquid (μm)	δ_0 deduced from experimental results: from matching T_w curve (μm)	Relevant length from simple theory $(vt_\theta)^\ddagger$ (μm)	Ratio δ_0 experimental $(vt_\theta)^\ddagger$	Operating conditions: pressure (kN/m^2)	Operating conditions: $(T_{sat} - T_b)$ (degC)	Operating conditions: $(\dot{q}/A)_{ave}$ (kW/m^2)	Operating conditions: ν ($m^2/s \times 10^{-6}$)	Fluid
T1	0·4	4·6	6·6	6·3	6·6	0·9	13·8	1·7	47·3	0·43	Toluene
	1·9	11·1	12·3	13·5	18·1	0·7					
	3·4	17·5	19·1	19·6	27·4	0·7					
	4·9			28·0	39·0	0·7					
T2	0·4	4·7	7·2		6·2	1·0	6·9	1·1	47·3	0·50	Toluene
	1·9	9·4	12·5		15·9	0·7					
	3·4	16·8	16·0		25·2	0·7					
	4·9	24·4	25·1		31·8	0·8					
T3	0·4	5·6	8·9		8·9	0·8	6·9	1·1	22·7	0·52	Toluene
	1·9	13·4	15·8		22·8	0·6					
	3·4			22·8	36·0	0·6					
	4·9			31·7	49·8	0·6					
T4	0·4	4·8	8·4		8·1	0·8	13·8	7·8	47·3	0·44	Toluene
	1·9	13·2	14·6		23·6	0·6					
	3·4			20·4	39·4	0·5					
	4·9										
T5	2·5		10·8		13·1	0·8	6·9	0	47·3	0·48	Toluene
	5·1		15·6		22·2	0·7					
	7·6		22·1		34·8	0·6					
	10·2		29·0		44·0	0·7					
T6	2·5		13·2		19·3	0·7	6·9	0	22·7	0·50	Toluene
	5·1		21·1		31·5	0·7					
	7·6			29·2	46·0	0·6					
	10·2			38·1	59·0	0·6					
T7	2·5		13·5		17·8	0·8	13·8	0	47·3	0·42	Toluene
	5·1		21·1		32·4	0·7					
	7·6			29·2	43·5	0·7					
	10·2			39·4	59·0	0·7					
I2	1·5			21·6	29·1	0·7	6·9	4·4	47·3	1·69	Isopropyl alcohol
	3·0			33·0	46·3	0·7					
	4·6			43·2	62·0	0·7					
	6·1			56·0	82·4	0·7					
I3	1·5			25·4	29·8	0·9	6·9	2·2	22·7	1·77	Isopropyl alcohol
	3·0			42·0	51·7	0·8					
	4·6			50·8	75·8	0·7					
	6·1										

heat needed for evaporation. After minor allowance for superheat in the microlayer when initially formed, this leads to a value "δ_0 from heat flow in solid", which is shown in col. 3 for all relevant cases.

Table 1, *col.* 4. The rate of evaporation from the microlayer depends on the rate of conduction of heat through it, and that depends on the temperature T_{int} at the liquid vapour interface. That differs from T_{sat}, the saturation temperature corresponding to the system pressure, due to the difference between bubble pressure and system pressure, arising mainly from surface tension and inertia forces in the liquid. Also, the finite rate of evaporation causes a temperature drop at the interface. These effects are discussed in [13] and shown to be small for the bubbles considered here, so T_{int} is taken to be T_{sat}.

In addition the thermal capacity of the microlayer can be neglected (i.e. $\rho_l C_p \delta (\partial T/\partial t) \ll k (\partial T/\partial x)$ in the microlayer) hence the temperature may be taken to vary linearly through the microlayer, so

$$-\rho_l h_{fg} \frac{\mathrm{d}\delta}{\mathrm{d}t} = k_l \frac{T_w - T_{sat}}{\delta}$$

hence

$$\delta_0^2 = \frac{2k_l}{\rho_l h_{fg}} \int_{t_g}^{t_e} (T_w - T_{sat})\,\mathrm{d}t$$

where t_g is the time when the bubble has grown to the point in question, and t_e is the time when the microlayer has evaporated completely there. The integral can be estimated readily from the temperature–time trace, and the resulting value, "δ_0 from heat flow in microlayer" is shown in col. 4 for all relevant cases.

Table 1, *col.* 5. A computer program was prepared which solved the combined equations for flow of heat in the solid and fluid, and thus determined the variation of the wall surface temperature for given initial temperature distribution in the solid and fluid and given initial microlayer thickness. The program was run with trial values of δ_0 to find that value which gave the best fit to the experimental temperature–time trace for stage 1. The resulting "δ_0 from matching T_w curve" is tabulated in col. 5, for all cases which were computed. Where the microlayer evaporated completely, this result agrees well with that in col. 4. Where the microlayer did not evaporate completely, this is the only estimate of δ_0 available. Since the program involved iteration, it demanded considerable computer time, so it was chiefly used for thermometers at which the microlayer did not evaporate completely, and also used for all thermometers of one run with toluene on glass and one run with toluene on ceramic.

The agreement between the three methods of calculating δ_0 is sufficiently close to support the microlayer theory.

Additional support is derived from the shape of the temperature–time curve, no. 3 of Fig. 2(b). The program used for stage 1 predicts variation of T_w in close agreement with that observed except towards the end of evaporation, when the program predicts a sharper fall than is observed. The sharp point in the theoretical curve is rounded off in practice, due to the size of the thermometer element and the failure of the simplifying assumptions that radial heat flow is negligible and that T_{int} equals T_{sat}. The additional possibility of motion in the microlayer is discussed in section 5.6 below.

As described in [1] and [13], similar comparisons of experiment with computer results were carried out, using other materials with different thermal and viscous properties, ceramic wall and isopropyl alcohol. Agreement was again sufficiently close to support the microlayer theory. Comparatively few runs were made with the ceramic wall because it introduced experimental difficulties. Its surface was not as smooth as glass, so the deposited thermometers had higher resistance, causing some electronic problems, leading to greater errors in temperature measurement. Those errors led to disproportionate errors in deduced heat flux because actual

changes in wall temperature were small. Also it was difficult to suppress unwanted nucleation of bubbles at the junction of tube and plate.

5.2 *Hydrodynamics of microlayer formation*

Since the processing of the temperature measurements strongly suggests that a microlayer is formed, at least for the cases observed, it is of interest to consider the hydrodynamics of formation of such layers.

If a bubble grows in a large body of liquid, remote from any solid boundaries, and if forces of inertia in the liquid predominate over other forces such as gravity, then the bubble grows as a sphere (Fig. 3). If a dividing wall is now

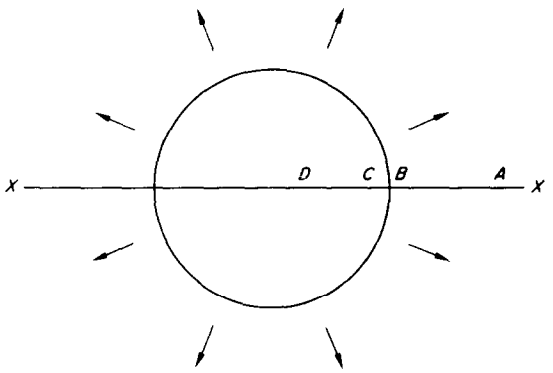

FIG. 3. Spherical or hemispherical bubble—location of points *A*, *B*, *C*, *D*.

assumed to exist at XX, at which the fluid velocity is zero, then the effect of the wall on the fluid outside the bubble is to bring to rest that fluid adjacent to the wall XX, and also to reduce the outward radial velocity of fluid in a limited region or boundary layer near to the wall. The thickness of this boundary layer is small compared to the bubble radius if the viscosity is suitably small. The velocity at a region such as A, well outside the bubble, is thus of the form sketched in Fig. 4(a). If the bubble is to sweep the wall dry, then by some means the fluid in the boundary must be accelerated to the general outward radial velocity. As will be shown below, that demands, for our cases, a strongly non-wetting liquid. If the liquid is not strongly

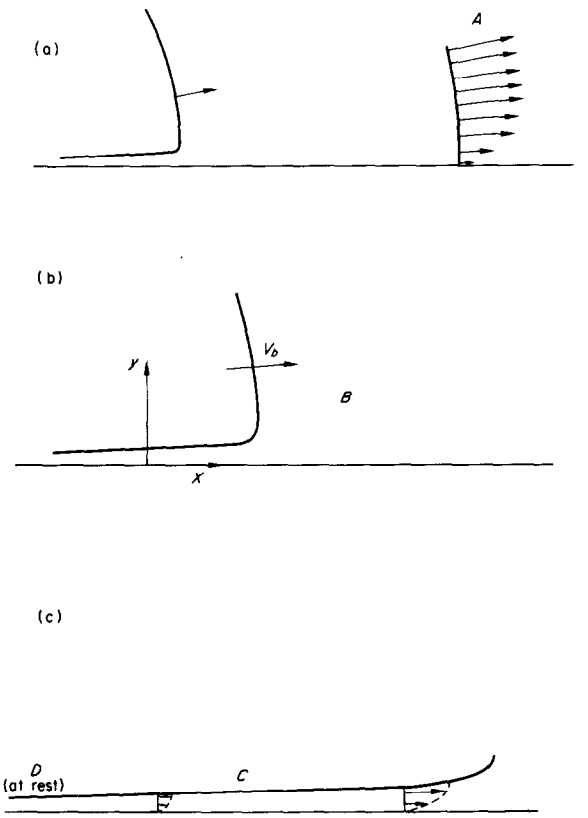

FIG. 4. Velocity fields at points *A*, *B*, *C*, *D*.

non-wetting then some of the liquid in the boundary layer gets "overtaken" by the growing bubble. Full analysis of the flow pattern would be very difficult particularly in region B (Fig. 4(b)], where the forces of inertia, viscosity and surface tension are all significant. However, reasonable agreement with the limited observations available can be obtained from certain simplified models. These are described in Appendix A, and lead to the expression for microlayer thickness

$$\delta_0 = C_2 \sqrt{(\nu t_g)}$$

where t_g is the time taken for the bubble to grow to the point considered, and C_2 is a constant of order 0·8.

To compare this theory with the experimental results obtained from the thermodynamic

reasoning of section 5.1, Table 1 has been extended by evaluating $\sqrt{(vt_g)}$ for all cases (col. 6) and evaluating the average of the experimental values for δ_0 and hence the ratio:

$$\frac{\delta_0 \text{ from experiment}}{\sqrt{(vt_g)}} \qquad \text{(col. 7)}$$

for these few results, the ratio is seen to lie in the range 0·5 to 1·0. The only other results known to the authors which give both microlayer thicknesses and time of growth are from [10], but there the hydrodynamics were altered by the presence of a microscope objective lens within the region of growth of the bubble, which probably affected the microlayer. For the results of [10], $\delta_0/\sqrt{(vt_g)}$ is in the range 0·3 to 0·5.

No firm conclusions can be drawn from these few data, and the theory outlined in Appendix A contains so many approximations that the agreement with observations may be partly due to cancellation of errors. It is to be hoped that more data will become available for other fluids and other conditions, but it is taken as a working hypothesis for this paper that $\delta_0 = 0{\cdot}8\sqrt{(vt_g)}$.

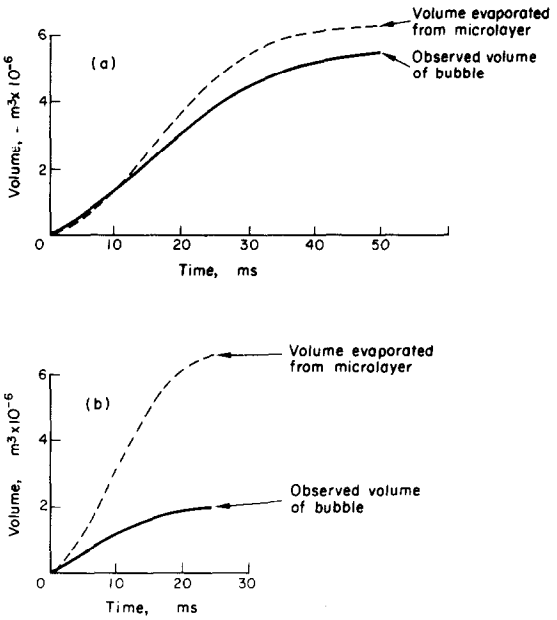

FIG. 5. Comparison of observed volume of bubble and computed volume evaporated from microlayer.
(a) Run 1, toluene on glass.
(b) Run 4, toluene on glass.

5.3 *The microlayer and bubble growth*

By applying the analysis of section 5.1 to the observed bubbles, it is possible to derive the initial thickness of the microlayer at all points and hence deduce its rate of evaporation at all points at all times during the lifetime of the bubble, and hence by integration deduce the volume of vapour evaporated from the microlayer and compare it with the observed size of the bubble. This has been done for two runs (nos. 1 and 4, toluene on glass) for the early part of bubble life, with the results shown in Fig. 5(a) and (b) where the dotted lines represent the volumes of vapour evaporated from the microlayer and the full lines represent the volumes of the bubbles determined from the high speed cine films. The bubbles were nearly hemispherical for the first 15 ms. In Fig. 5(a) the actual growth rate is seen to be similar to that due to evaporation of the microlayer, reflecting the fact that the temperature of the bulk liquid was nearly at the saturation temperature whereas in Fig. 5(b) the actual growth rate was much slower, due to the bulk temperature being some 10°C below the saturation temperature. The net rate of evaporation and condensation over the curved surface of the bubble was small in Fig. 5(a) and large (condensation) in Fig. 5(b). Clearly the evaporation from the microlayer is a significant factor in these cases. As shown in Appendix B, this rate of evaporation can be expressed analytically provided the expression $\delta_0 = 0{\cdot}8\sqrt{(vt_g)}$ is accepted, and the bubble grows in accordance with a power law $R = C_1 t^n$ with known C_1 and n. The calculations described above amount to analysis of an observed growth rate, whereas prediction of growth rate would be more useful.

There are several current theories predicting rate of growth of bubbles. Plesset and Zwick [14] and Scriven [15] consider growth in a liquid initially at uniform temperature. Other cases are considered by Zuber [16], Hsu and

Graham [17], and Han and Griffith [18]. In some cases predictions can be derived which agree quite well with the observed rates of growth of these bubbles, though they take little or no account of microlayer evaporation.

To predict growth of bubbles allowing for microlayer evaporation it is necessary to know the thickness of that layer. That may reasonably be taken to be $\delta_0 = 0{\cdot}8\sqrt{(vt_g)}$, but there appears to be a contradiction here, in that it appears necessary to know the growth time t_g in order to predict the growth of the bubble. However, the growth of a bubble under specific conditions can be predicted by a computer program which proceeds step by step, determining values of t_g and hence δ_0 for increasing radii as the bubble grows. As shown in Appendix C the program can also allow for evaporation or condensation over the curved surface of the bubble in accordance with Fig. 6. When applied to the two

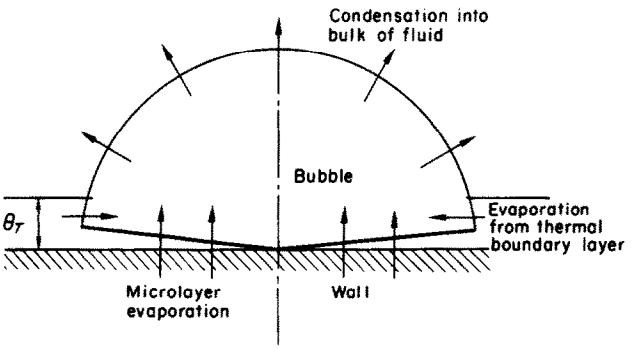

FIG. 6. Model for bubble growth.

bubbles represented in Fig. 5(a) and (b) the results are as shown in Fig. 7(a) and (b). For the second bubble, growing in subcooled liquid, there was a significant amount of condensation over the curved surface of the bubble, leading to a slower growth, as predicted by the program.

5.4 *Bubble shape*

The theories developed in Appendixes A and B for the formation of a microlayer and the growth of a bubble depend on the assumption that the bubble is nearly hemispherical in shape during growth. That assumption is nearly

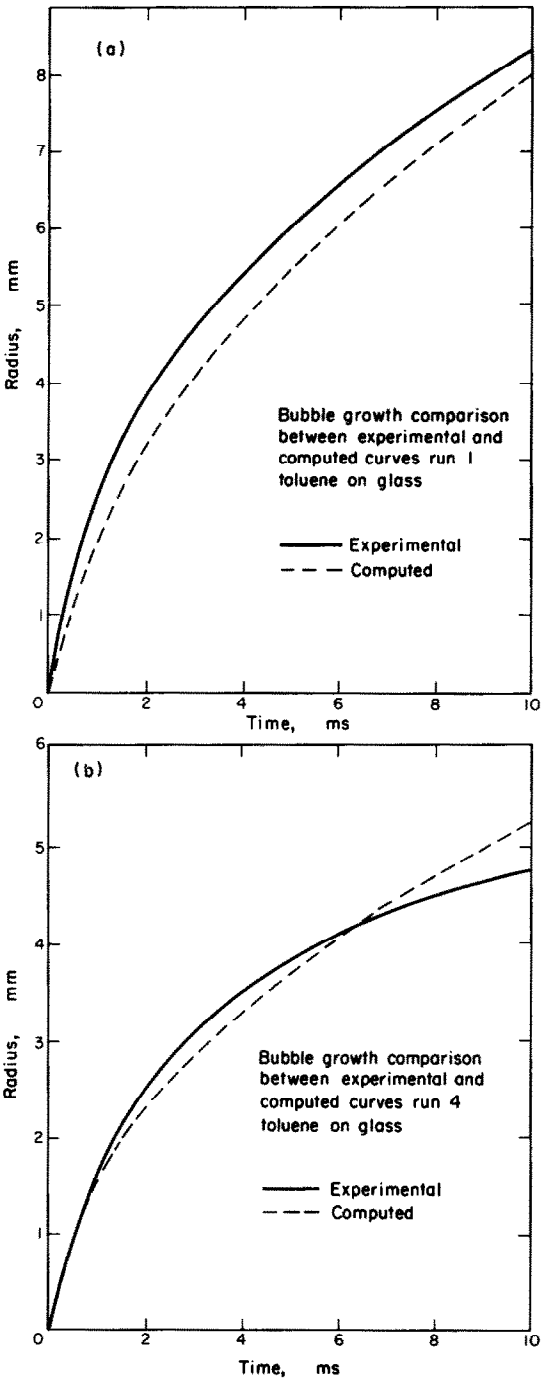

FIG. 7. Bubble growth—comparison between experimental and computed curves.
(a) Run 1, toluene on glass.
(b) Run 4, toluene on glass.

correct for the bubbles reported here, but other experimenters [18, 19] report a variety of shapes including nearly complete spheres, slightly flattened at contact with the wall. The theories of Appendixes A and B would not apply and the area available for any microlayer to form on the wall would be reduced. Furthermore, there may be cases in which the forces preventing the bubble from growing as a hemisphere are such as to prevent the formation of any micro-layer.

Johnson *et al.* [19] present photographs of bubbles produced under a wide range of conditions. They classify them as spherical, hemispherical and oblate, and suggest that the shape is determined by the relative sizes of the contributions of inertia and surface tension to the equation for the excess pressure inside the bubble. If the former term predominates (as in a rapidly growing bubble) they suggest that a bubble growing on a flat surface will be nearly hemispherical. If the latter term predominates, they suggest that the bubble will tend towards a spherical shape. In an attempt at quantitative verification of these suggestions, the terms have been evaluated below for two bubbles, as follows:

inertia term $$P_i = \rho_l\left(R\ddot{R} + \frac{3}{2}\dot{R}^2\right)$$

surface tension term $P_s = 2\dfrac{\sigma}{R}$.

In addition, two further terms have been formulated to represent the contributions of viscous and gravitational stresses. These are:

viscous term $$P_v = 4\mu\frac{\dot{R}}{R}$$

gravitational term $P_g = (\rho_l - \rho_v)\,gR$.

The basis for these terms is discussed in Appendix D. They can be evaluated as functions of time, if the bubble radius R is known as a function of time.

For tests 1–4 with toluene boiling on glass, the radius was very nearly proportional to (time)$^{\frac{1}{2}}$. Test 1 was typical, with $R = 0{\cdot}084\ t^{\frac{1}{2}}$ and the terms have been evaluated for this, with the results shown in Fig. 8. The inertia term predominated throughout the growth period, so a hemispherical shape is to be expected, and that was observed in the photographs.

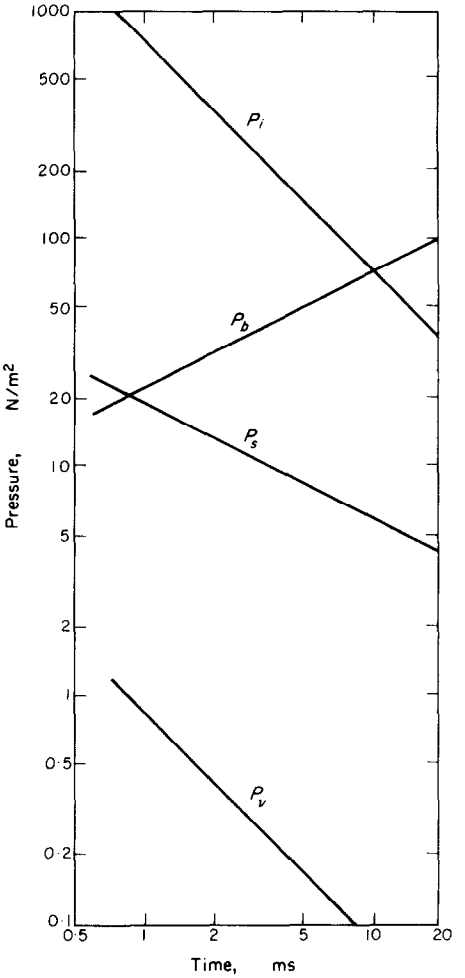

FIG. 8. Comparison of pressure terms defined in Appendix A, for run 1, toluene on glass.

For the tests with water described in [18] the bubbles did not grow hemispherically and the radii reported do not conform to any power law. For bubble 2 an attempt has been made to assess the pressure terms by simple numerical differentiation, but the double differentiation

needed for P_i leads to erratic values. However, it is clear that P_s predominates over P_i by a factor of about five, except perhaps for the first fraction of a millisecond, so a more nearly spherical shape is to be expected. The photographs show the bubble is of intermediate shape, having a base area in apparent contact with the wall rather less than it would be for a hemispherical bubble. The base area grows to its final value within 3 or 4 ms, whereas the bubble continues to grow for several times as long. Nevertheless, the base area is an appreciable fraction of the whole area of the bubble for most of the lifetime of the bubble. The gravity term remains small.

In both cases the viscous term P_v is much smaller than the predominant term.

Factors tending to make bubbles grow rapidly to large size will tend to encourage formation of a microlayer and also make the bubble of hemispherical shape, with a large area of contact at the wall, hence a large area of microlayer. Intuitively one would expect such factors to include:

High wall temperature, encouraging flow of heat into the bubble from the wall and the thermal boundary layer. High heat flux and smooth surface will tend to raise wall temperature.

High bulk temperature, encouraging growth of bubbles, whereas subcooling tends to reduce bubble size by condensation. Low system pressure, increasing the specific volume of vapour.

5.5 *Bubble departure*

These experiments shed no further direct light on the phenomena of bubble departure, but the experiments emphasise the importance of the hemispherical bubble shape which occurs when a bubble grows at a wall with the forces of inertia in the liquid greatly outweighing the forces due to viscosity, surface tension, buoyancy and motion of the gas phase. It is worth noting that if the forces due to viscosity, surface tension, buoyancy, and motion of the gas phase are all negligible, then there is no tendency for the bubble to depart when it stops growing. The departure must be due to significant changes in the flow pattern arising from the phenomena excluded above (and departure even occurs when buoyancy is negative) or other phenomena such as thermocapillarity. To prove this statement, we consider the dynamics of flow of the liquid surrounding such a bubble and compare it with the dynamics of the flow in the liquid surrounding a spherical bubble growing in an infinite mass of liquid (Fig. 3). If inertia predominates, the two are identical radial motions. The spherical bubble has, of course, no tendency to move as its rate of growth changes or stops. But motion of a bubble is determined by motion of the liquid surrounding it. Hence the hemispherical bubble also has no tendency to move. False conclusions about motion of a hemispherical bubble due to inertia alone can be reached by certain arguments based on the concept of effective inertia assumed to apply to the bubble and applied to its moving centroid, or by arguments based on the concept of overall momentum in the liquid, which are apt to ignore the force applied to the liquid by the varying pressure at the wall. Such arguments must therefore be treated with reserve when applied to bubbles of other shapes.

5.6 *Wettability*

So far, the analysis has sidestepped the effects of wettability of the liquid–solid combination. The triple interface between solid, liquid and vapour at which this arises has been "left behind" under the bubble. Motion of such triple interfaces does not seem to be fully understood.

There is a possibility that the microlayer might subsequently "roll up" from the dry inner region under the action of surface forces, thus increasing the dry area, even without any evaporation. However, the observations reported here suggest that it is not happening to any great extent in these experiments, otherwise there would be greater divergence between the observed and calculated values of temperature

towards the end of stage 1. It may be more likely to happen if microlayer evaporation is slow. More experimental work would be useful, and a related simpler problem is the motion of thin liquid films under isothermal conditions, though in boiling there may be additional effects due to variation of surface tension caused by variation in concentration of impurities or by variation of interface temperature, introducing additional complications.

Another more extreme possibility is that the advancing bubble would dry out the solid surface, preventing formation of a microlayer. From Fig. 4(b) it appears that the momentum deficit due to the velocity deficit in the viscous boundary layer of the liquid would have to be made up by the advancing interface producing a force in the advancing direction. Such a force $\sigma\cos\theta$ is produced if the solid, liquid, vapour combination has a non-wetting contact angle θ even at these rapid rates of advance. This kind of behaviour is very sensitive to the presence of impurities at the interface and other phenomena apparently not understood, but it appears that a sufficiently strongly non-wetting combination of liquid and solid could produce a force equivalent to the momentum deficit occurring in the bubbles studied here. However, the experiments reported here did not use strongly non-wetting liquids, because it was essential to have low electrical conductivity, and the liquids of this type available were organic, having small contact angle on glass.

6. CONCLUSIONS

Under certain circumstances, an isolated vapour bubble growing at a heated wall apparently has beneath it a thin liquid layer, the microlayer, which evaporates rapidly and affects the growth of the bubble. Factors tending to promote the formation of the microlayer are: high wall temperature, high bulk temperature and low system pressure.

A simplified hydrodynamic theory predicts that the thickness of the microlayer is $0{\cdot}8\sqrt{(vt_g)}$, and experimental observations indicate thicknesses in the range $0{\cdot}5$ to $1{\cdot}0\sqrt{(vt_g)}$.

Consideration of the effects of microlayer evaporation on growth of the bubble suggests that such effects are significant for the bubbles reported here. Under certain assumptions the rate of evaporation from the microlayer can be expressed in closed analytic form. For other cases, a step by step method has been developed to predict the growth of a bubble, making allowance simultaneously for evaporation from the microlayer and evaporation or condensation on the remainder of the bubble surface. The results are in reasonable agreement with observed rates of growth. (± 15 per cent).

ACKNOWLEDGEMENTS

The work described here was supported in part by the Central Electricity Research Laboratories of the Central Electricity Generating Board.

One author (A.J.P.L.) acknowledges receipt of a grant from the Scientific Research Council.

REFERENCES

1. M. G. Cooper and A. J. P. Lloyd, Transient local heat flux in nucleate boiling, *3rd Int. Heat Transfer Conf.*, paper 100, Chicago (1966).
2. S. T. Hsu and F. W. Schmidt, Measured variations in local surface temperatures in pool boiling of water, *Trans. Am. Soc. mech. Engrs*, Ser C, **83**, 254 (1961).
3. F. D. Moore and R. B. Mesler, The measurement of rapid surface temperature fluctuations during nucleate boiling of water, *Trans. Am. Inst. chem. Engrs* **7**, 620 (1961).
4. T. F. Rogers and R. B. Mesler, An experimental study of surface cooling by bubbles during nucleate boiling of water, *Trans. Am. Inst. chem. Engrs* **10**, 656 (1964).
5. R. C. Hendricks and R. R. Sharp, Initiation of cooling due to bubble growth on a heating surface, NASA TN D-2290 (1964).
6. N. R. Snyder and D. K. Edwards, Post conference comments: summary of conference on bubble dynamics, Memo 20-137 Jet Propulsion Laboratory (1956).
7. R. R. Sharp, The nature of liquid film evaporation during nucleate boiling, NASA TN D-1997 (1964).
8. K. Torikai, M. Hori, M. Akiyama, T. Kobori and H. Adachi, Boiling heat transfer and burnout mechanism in boiling water cooled reactor, 3rd U.N. Int. Conf. on the peaceful uses of Atomic Energy, A/Conf., 28/P/580 (1964).
9. N. B. Hospeti and R. B. Mesler, Deposits formed beneath bubbles during nucleate boiling of radioactive calcium sulfate solution, *Trans. Am. Inst. chem. Engrs* **11**, 663 (1965).

10. Y. KATTO and S. YOKOYA, Experimental study of nucleate pool boiling in case of making interference plate approach to the heating surface, *3rd Int. Heat Transfer Conf.*, paper 103 Chicago (1966).
11. C. BONNET, E. MACKE and R. MORIN, Visualisation de l'ebullition nucléée de l'eau a pression atmospherique et mesure simultanee des variations de temperature de surface, EUR 1622f (1964).
12. M. G. COOPER and A. J. P. LLOYD, Miniature thin film thermometers with rapid response, *J. scient. Instrum.* **42**, 791 (1965).
13. A. J. P. LLOYD, Ph.D. Thesis, Cambridge University, England (1966).
14. M. S. PLESSET and S. A. ZWICK, The growth of vapour bubbles in superheated liquids, *J. appl. Phys.* **25**, 493 (1954).
15. L. E. SCRIVEN, On the dynamics of phase growth, *Chem. Engng Sci.* **10**, 1 (1959).
16. N. ZUBER, The dynamics of vapour bubbles in non-uniform temperature fields, *Int. J. Heat Mass Transfer* **2**, 83 (1961).
17. Y. Y. HSU and R. W. GRAHAM, An analytical and experimental study of the thermal boundary layer and ebullition cycle in nucleate boiling, NASA TN D-594 (1961).
18. C-Y. HAN and P. GRIFFITH, The mechanism of heat transfer in nucleate pool boiling, *Int. J. Heat Mass Transfer* **8**, 887 (1965).
19. M. A. JOHNSON, J. DE LA PENA and R. B. MESLER, Bubble shapes in nucleate boiling, *J. Am. Inst. chem. Engrs* **12**, 344–348 (1966).
20. H. S. CARSLAW and J. C. JAEGER, *Conduction of Heat in Solids*, 2nd Edn, Oxford University Press, London (1959).

APPENDIX A

Hydrodynamics of Microlayer Formation

In this appendix, simple models are used to discuss the behaviour of liquid inside a microlayer and also outside a growing bubble, leading to a relationship for the thickness of the microlayer.

In the experiments reported above, the thicknesses of the microlayer and the viscous boundary layer in the liquid were both small compared with the radius of the bubble, so the flow is here regarded in the first instance as plane (two-dimensional) [Fig. 4(b)].

In addition, for the flow in the microlayer the pressure is taken to be uniform since the liquid–vapour interface is nearly plane. Also the layer is so thin that the situation is typical of lubrication problems in that the derivatives in the x direction can be neglected. This leads to the Navier Stokes equation for the velocity U in the x direction

$$\nu \frac{\partial^2 U}{\partial y^2} = \frac{\partial U}{\partial t}.$$

If the boundary condition at the liquid–vapour interface $y = \delta$ is zero shear (i.e. surface tension is constant), then this equation can be solved by separation of variables, leading to:

$$U = \sum_{m=1}^{\infty} \left\{ U_m \sin (2m + 1) \frac{\pi}{2} y \times \exp. \left(-(2m + 1)^2 \frac{\pi^2}{4} \frac{\nu t}{\delta^2} \right) \right\}.$$

Higher order terms decay away rapidly, leaving the first term predominant, but it too decays away in a time of order (δ^2/ν) and the liquid may be regarded as being at rest at a region D (Fig. 4(c)) to be further considered below.

To approximate to the flow across region B, we again assume plane two dimensional flow, and also apply to the flow patterns of Fig. 4 a velocity U_b equal and opposite to the bubble growth rate. This gives the flow pattern shown in Fig. 9, with a nearly stationary interface, and a straight wall moving with velocity U_b parallel to its length, and with fluid velocities $U'(y, t)$ differing by U_b from those of the original problem. On the left, in the region corresponding to D of Fig. 4(c), the fluid velocity U' is equal to U_b. A major assumption which is now introduced is that the rate of flow into the right of Fig. 9 is equal to the flow out of the left. If that is accepted as a plausible approximation, then we have

$$\delta_0 U_b = \int_0^{\infty} U' \, dy = \int_0^{\infty} (U - U_b) \, dy$$

or, in terms of boundary layer theory, δ_0 is equal to the displacement thickness θ_d of the boundary layer of Fig. 4(a). To determine θ_d the flow pattern for U' is taken to be that which would arise in a semi-infinite mass of liquid if an

appropriate velocity U_w were applied to the wall. In this configuration the Navier–Stokes equation for the x direction again reduces to

$$\nu \frac{\partial^2 U}{\partial y^2} = \frac{\partial U}{\partial t}$$

and the solution depends, of course, on the variation of U_w with time. That variation depends on the rate of growth of the bubble, for which the three dimensional picture must again be considered. Many experimenters suggest that bubble radius R grows as

$$R = C_1 t^n$$

with values of n generally in the range 0·3 to 0·7. This leads to an expression for the bubble volume V and its rate of growth:

$$\frac{dV}{dt} = 2\pi C_1^3 n t^{3n-1}$$

so the velocity at a point at radius r, well outside the bubble is:

$$\frac{C_1^3 n t^{3n-1}}{r^2} = C' t^{3n-1}$$

for given r.

Putting $U_w = C' t^{3n-1}$ and in particular taking $n = 0{\cdot}5$, in line with the experiments reported here, we obtain from Carslaw and Jaeger [20]:

$$U' = U_w \sqrt{\pi}\, \text{ierfc}[y/2\sqrt{(\nu t)}]$$

and

$$\int_0^\infty U'\, dy = \tfrac{1}{2}\sqrt{\pi}\,\sqrt{(\nu t)}\, U_w.$$

But when the bubble passes the point in question, $U_w = U_b$, hence:

$$\delta_0 = \tfrac{1}{2}\sqrt{\pi}\,\sqrt{(\nu t_g)}$$

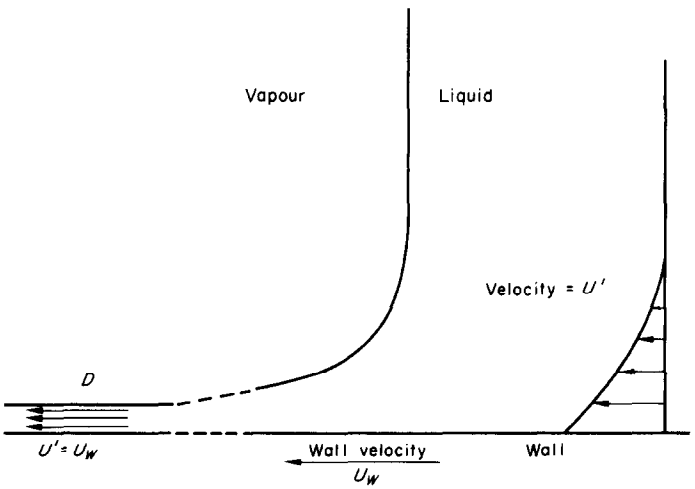

FIG. 9. Fluid velocities relative to frame of reference moving at velocity of bubble growth.

where t_g is the time for the bubble to grow to the point in question.

It is necessary to consider the mean distance travelled by the liquid in the microlayer in the region between B and D, while slowing down. If in Fig. 10 the full line above point P represents marked particles of fluid above P just after the microlayer forms there, then these particles will be distributed to the right of P when the

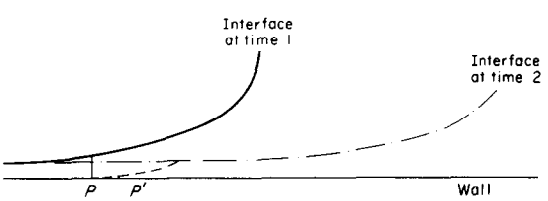

FIG. 10. Motion of microlayer beneath bubble.

microlayer comes to rest relative to the wall, as shown by the dotted line in Fig. 10. Hence the value of θ_d as the microlayer forms at P will be related to the thickness of the microlayer δ_0 at some mean point P' to the right of P. If θ_d is constant, then the difference between P and P' is immaterial in the plane flow pattern. However, in the actual case of outward radial motion, the distance PP' corresponds to an increase in the radius at which the layer is deposited so continuity demands a corresponding reduction in microlayer thickness by

$$\frac{r}{r + PP'}.$$

To estimate PP'/r we use the earlier analysis of flow in the microlayer taking only the first term in the series:

$$U = U_1 \sin(\tfrac{1}{2}\pi y) \exp.\left(-\frac{\pi^2}{4}\frac{vt}{\delta^2}\right)$$

and take the mean of the distance travelled for $t > 0$. This is

$$PP' = \frac{1}{\delta}\int_{t=0}^{\infty}\int_{y=0}^{\delta} U \,\mathrm{d}y\,\mathrm{d}t = \frac{8}{\pi^3}\frac{\delta^2}{v}U_1.$$

Substituting δ_0 for δ

$$PP' = \frac{2}{\pi^2}U_1 t_g.$$

To relate this to r we need to know U_1, a scale factor for the initial velocity pattern at P. Here it is assumed that U_1 is equal to $\dot{R}$, the bubble growth velocity.
i.e.

$$U_1 = \frac{\mathrm{d}}{\mathrm{d}t}(C_1 t^n)$$

$$= nC_1 t^{n-1} = n\frac{R}{t_g}$$

$$= \tfrac{1}{2}\frac{R}{t_g} \qquad \text{taking } n = \tfrac{1}{2}.$$

Hence $PP' = \dfrac{R}{\pi^2}$ or approx. 0·1 R.

In the present state of the theory, this is a very small correction to consider. However, it is easily incorporated here, and leads to a revised value of the effective initial microlayer thickness:

$$\delta_0 = \frac{\pi^2}{\pi^2 + 1}\frac{\sqrt{\pi}}{2}\sqrt{(vt_g)}$$

$$= 0{\cdot}8\sqrt{(vt_g)}.$$

In [13] a more accurate analysis of the development of the boundary layer is given, allowing for the true spherical geometry and for convective terms, and leading to a value of C_2 some 40 per cent larger. However, as explained in this paper, a value 0·8 is in better agreement with available experimental results, possibly due to cancellation of errors.

An analysis of the case $n \neq \frac{1}{2}$ is also given in [13].

As discussed in section 5.6, there is a possibility that forces of surface tension at the triple interface may cause greater movement of the liquid in the microlayer in some cases.

APPENDIX B

Rate of Evaporation from the Microlayer

The rate of evaporation from the microlayer is needed, not only to determine its contribution to bubble growth rates, but also to determine rates of mass transfer across a bubble of known growth rate. An analytic expression can be derived for the volume of vapour evaporated from the microlayer as a function of time on the following assumptions:

(1) The bubble grows hemispherically with radius given by:

$$R = C_1 t^n.$$

(2) The initial thickness of the microlayer at any point is:

$$\delta_0 = C_2\sqrt{(vt_g)}$$

where C_2 is a function of n only.

(3) The wall temperature is nearly constant during most of the period of evaporation of the microlayer.

(4) The initial temperature profile in the liquid is linear.
(5) The temperature at the liquid to vapour interface is nearly equal to the saturation value at system pressure.
(6) The thermal capacity of the liquid in the microlayer is negligible.

If at time t the microlayer has dried out as far as radius r_e and had thickness $\delta(r)$ for greater radii, then the volume V_m of vapour which has been formed by evaporation of the microlayer is given by:

$$V_m = \frac{\rho_l}{\rho_v}\left\{\int_0^{r_e} \delta_0 2\pi r \, dr + \int_{r_e}^{R} (\delta_0 - \delta) 2\pi r \, dr\right\}$$

$$= 2\pi \frac{\rho_l}{\rho_v}\left\{\int_0^{R} (\delta_0) r \, dr - \int_{r_e}^{R} (\delta) r \, dr\right\}$$

where, from equation (2) with T_w constant

$$\delta = \left\{\delta_0^2 - \frac{2k_l}{\rho_l h_{fg}}(T_w - T_{sat})(t - t_g)\right\}^{\frac{1}{2}}$$

$$= \{\delta_0^2 - C_3(t - t_g)\}^{\frac{1}{2}} \text{ where } C_3 = \text{a constant}$$

employing assumptions 1 and 2 above, this can be written:

$$\delta = \left\{\frac{C_2^2 v + C_3}{C_1^{1/n}}\right\}^{\frac{1}{2}} \left\{r^{1/n} - \frac{C_3}{C_2^2 v + C_3} R^{1/n}\right\}^{\frac{1}{2}}$$

But r_e is that value of r for which $\delta = 0$, hence:

$$r_e = \left\{\frac{C_3}{C_2^2 v + C_3}\right\}^{n} R$$

showing that, for this special case, the dried out radius is a constant fraction of the bubble radius during growth. We may now write

$$\delta = C_4(r^{1/n} - r_e^{1/n})^{\frac{1}{2}} \text{ where } C_4 = \left\{\frac{C_2^2 v + C_3}{C_1^{1/n}}\right\}^{\frac{1}{2}}$$

Substituting this expression and assumptions 1, 2 into the expression for V_m we obtain

$$V_m = 2\pi \frac{\rho_l}{\rho_v}\left\{\int_0^{R} \left[\frac{C_2^2 v}{C_1^{1/n}} r^{1/n}\right]^{\frac{1}{2}} r \, dr\right.$$

$$\left. - \int_{r_e}^{R} C_4(r^{1/n} - r_e^{1/n})^{\frac{1}{2}} r \, dr\right\}$$

which can be evaluated.
The solution is particularly simple if $n = \frac{1}{2}$, leading to:

$$V_m = \frac{4\pi}{3} \frac{C_1^2 C_2 k_l (T_w - T_{sat}) v^{\frac{1}{2}} t^{\frac{3}{2}}}{\rho_v h_{fg} C_2^2 v + 2k_l (T_w - T_{sat}) \rho_v / \rho_l}$$

It can be seen that for this case the evaporated volume is proportional to $t^{\frac{3}{2}}$. Thus for a bubble of constant shape the ratio of evaporated volume to total volume would be constant with respect to time.

If evaporation from the thermal boundary layer is neglected, the mass transfer across the bubble can be determined by observing that the condensation on the curved surface of the bubble is the difference between the total volume of the bubble and this expression for the evaporation from the microlayer.

APPENDIX C

Bubble Growth

An approximate computer program has been developed and applied to the toluene bubbles nos. 1 and 4. As shown in Fig. 2, they have widely different growth patterns, although the only difference in conditions is that for one of them the bulk liquid was near to saturation temperature, while for the other it was appreciably subcooled.

The program uses a step by step process to determine t_g and hence δ_0 for increasing radii as the bubble grows, and hence determine evaporation from the microlayer at any time. The program also allows for evaporation or condensation over the curved surface of the bubble in accordance with the model shown in Fig. 6, but in its present form the program is not intended to describe accurately the processes of bubble initiation and early growth. It ignores the effects of changes in bubble pressure upon

T_{sat}. Also the calculation starts by assuming the existence of a hemispherical bubble of radius much less than the thickness θ_T of the thermal boundary layer. Both of these assumptions concern early bubble history and have little effect on the prediction of subsequent growth of the large bubbles considered here.

In this program, θ_T is calculated by assuming one dimensional heat conduction in it. Hence, if $(\dot{q}/A)$ is the time average heat flux from the wall,

$$\theta_T = \frac{k_l(T_w - T_b)}{(\dot{q}/A)}.$$

After a very short initial period, the bubbles considered extend well out beyond the thermal boundary layer. Evaporation from the thermal boundary layer is then small, and it is given with sufficient accuracy by regarding the thermal boundary layer as a body initially at uniform temperature equal to the mean of T_w and T_b, brought into contact with a perfect conductor at temperature T_{sat} over area $2\pi r\theta_T$, regarded as a nearly plane boundary. This implies heat flow $\dot{q}_1$ given by:

$$(\dot{q}_1/2\pi r\theta_T) = k_l \frac{\frac{1}{2}(T_w + T_b) - T_{sat}}{(\pi\alpha t)^{\frac{1}{2}}}.$$

The heat flow q_2 between the bubble and the liquid over the remainder of the bubble surface (area A_s) is larger, so greater accuracy is needed and the analysis of Scriven [15] is used, giving approximately:

$$(\dot{q}_2/A_s) = 3^{\frac{1}{2}}k_l \frac{T_{sat} - T_b}{(\pi\alpha t)^{\frac{1}{2}}}.$$

The corresponding rates of evaporation are: $(\dot{q}_1(v_g - v_f)/h_{fg})$ and $(\dot{q}_2(v_g - v_f)/h_{fg})$.

The total rate of evaporation into the bubble is found by adding these to the evaporation from the microlayer, which is determined from the known values of δ_0 and evaporation for all radii, as described at the start of section 5.3.

The process is a lengthy one, and clearly needs amendment if it is to be used widely, but it was applied to the two bubbles shown in Fig. 5, with the results shown in Figs. 7(a) and (b). The program gives the correct order of magnitude for the effect of subcooling.

APPENDIX D

When a spherical gas bubble of radius R grows in a large mass of liquid remote from solid boundaries, the Navier–Stokes equations in spherical polar coordinates reduce to nil except in the radial direction, from which we deduce that the pressure in the liquid just outside the interface exceeds the pressure at infinity by:

$$\rho_l(R\dot{R} + \tfrac{3}{2}\dot{R}^2).$$

This shows that viscosity has no effect on the pressure, as expected for this irrotational, incompressible flow. However, due to the anisotropic strain, viscosity introduces anisotropic terms in the normal stress. The spherical coordinate axes (r, θ, ϕ) are principal axes of the tensors of strain and stress, hence:

$$e_{rr} = \frac{\partial u}{\partial r} = -2\frac{\dot{R}R^2}{r^3} = -2\frac{u}{r}; \quad e_{\theta\theta} = \frac{u}{r} = e_{\phi\phi}$$

where u is radial velocity. So

$$T_{rr} = -p - 4\mu\frac{\mu}{r}; \quad T_{\theta\theta} = -p + 2\mu\frac{u}{r} = T_{\phi\phi}.$$

At the liquid–gas interface there is the usual discontinuity in normal stress, $(2\sigma/R)$ so the pressure in the bubble exceeds the pressure at infinity by:

$$\rho_l(R\dot{R} + \tfrac{3}{2}\dot{R}^2) + 4\mu\frac{\dot{R}}{R} + 2\frac{\sigma}{R}.$$

These are the terms designated P_i, P_v, P_s.

The term $P_g(=(\rho_l - \rho_v)gR)$ can be regarded either as a typical hydrostatic pressure difference, or as the buoyancy force on the bubble, divided by a typical area.

These terms have been developed for a spherical bubble remote from walls, whereas the aim is to compare the relative influences of inertia, viscosity, surface tension and buoyancy

in determining the shape of a bubble growing near a wall. The viscous term should therefore relate to the tendency of the fluid near the wall to be restrained and prevented by viscous stresses from moving freely outward, thus forming a thick boundary layer. But the expression $(\mu\dot{R}/R)$ meets that requirement too, as it is the viscous stress which would arise if the liquid formed a boundary layer of thickness R and linear velocity profile. If that hypothetical stress is small compared with the inertia stresses, then the boundary layer will in fact be small compared with R. Similarly, the surface tension term P_s should perhaps be modified for hemispherical bubbles by relating it to the radii of curvature near the rim of the bubble [region B of Fig. 4(b)]. However, it too is retained in the form given above because the comparison of P_s with P_i is a measure of the extent to which the bubble can distort, since a small value of P_s/P_i indicates that large distortion can occur without surface tension introducing stresses comparable with the inertia stresses.

Résumé—On décrit des expériences dans lesquelles des liquides organiques subissent und ébullition en réservoir à faible pression, en formant de grandes bulles de vapeur sur la surface d'une plaque chauffante en verre ou en céramique. La température de la surface du chauffoir a été mesurée, conduisant à confirmer l'hypothèse qu'une couche mince de liquide (la microcouche) se forme sous la bulle de vapeur.

Il est possible de déduire, à partir des observations expérimentales, l'épaisseur de la microcouche, qui peut aussi être prédite à partir d'une théorie simple pour l'hydrodynamique de la formation de la couche. L'expérience et la théorie sont d'accord à ± 25 pour cent près pour les cas limités disponibles.

On montre que les vitesses de croissance des bulles sont du même ordre que les vitesses d'évaporation à partir des microcouches, qui peuvent être exprimées sous forme analytique avec certaines hypothèses.

Un programme de calculateur pour la croissance des bulles tenant compte de la microcouche et d'autres facteurs a été exploité et appliqué à deux bulles croissant avec des températures globales largement différentes. Les rayons prévus sont à ± 15 pour cent de ceux observés.

Les grandeurs relatives des contraintes dues à l'inertie, à la tension superficielle, à la viscosité et à la gravitation sont déterminées pour une bulle typique, et discutées en relation avec la forme de la bulle et avec la formation de la microcouche.

On a insisté sur le fait que ces résultats ne peuvent pas s'appliquer à des conditions d'ébullition largement différentes.

Zusammenfassung—Es wird über Versuche berichtet, bei denen organische Flüssigkeiten unter Bildung von grossen Dampfblasen an der Oberfläche einer beheizten Platte aus Glas oder Keramik dem Sieden in freier Konvektion bei niederem Druck unterzogen wurden. Die Oberflächentemperatur des Heizeelements wurde gemessen, weil sie massgebend für die Aufrechterhaltung der Hypothese ist, dass dich unter der Blase eine dünne Flüssigkeitsschicht (Mikroschicht) bildet.

Aus experimentellen Beobachtungen ist es möglich, auf die Dicke der Mikroschicht zu schliessen, die auch über eine einfache Theorie für die Hydrodynamik der Schichtbildung berechnet werden kann. Für die wenigen vorliegenden Fälle ergeben sich zwischen Experiment und Theorie Abweichungen von ± 25 Prozew.

Es zeigt sich, dass die Wachstumsraten der Blasen von derselben Grössenordnung wie die Verdampfungsraten der Mikroschichten sind, die unter gewissen Voraussetzungen in analytischer Form dargestellt werden können. Ein Rechenprogramm für das Blasenwachstum wurde unter Berücksichtigung der Mikroschicht und anderer Faktoren entwickelt und auf zwei Blasen, die bei sehr verschiedenen Flüssigkeitstemperaturen entstehen, angewendet. Die berechneten Radien stimmen auf ± 15% mit den beobachteten überein.

Die bezogenen Grössen für die Trägheitskraft, Oberflächenspannung, Zähigkeit und Schwerkraft werden für eine typische Blase bestimmt und im Zusammenhang mit der Blasenform und Mikroschichtbildung diskutiert.

Es wird mit Nachdruck darauf hingewiesen, dass diese Ergebnisse nicht auf zu sehr abweichende Seidezustände angewendet werden dürfen.

Аннотация—В статье описываются результаты экспериментов по кипению в большом объеме органических жидкостей при низком давлении при образовании больших пузырьков пара на поверхности стеклянной или керамической пластины — нагреван-

теля. Для проверки гипотезы об образовании тонкого слоя жидкости (микрослоя) под пузырьком пара измерялась температура поверхности нагревателя.

На основе экспериментальных наблюдений можно получить значение толщины микрослоя, которое, кроме того, может быть рассчитано с помощью простой гидродинамической теории образования слоя. Для рассмотренных случаев экспериментальные и теоретические результаты согласуются с точностью до $\pm 25\,\%$.

Показано, что скорость роста пузырьков имеет тот же порядок, что и скорость испарения из микрослоев. Разработана вычислительная программа для определения роста пузырьков с учетом микрослоя и других факторов. Эта программа применялась для случая двух пузырьков с различными объемными температурами. Расчетные и экспериментальные значения совпадают с точностью $\pm 15\,\%$.

Для типичного пузырька найдены относительные значения напряжений, обязанных инерции, поверхностному натяжению, скорости и силе тяжести, которые рассматриваются в связи с формой пузырька и образованием микрослоя.

Особо подчеркивается, что эти результаты легко применить к различным условиям кипения.